Thermo-reversible gelation of self-assembled conducting polymer colloids

Vidhika S. Damani,[1] Xinran Xie,[2] Rachel E. Daso,[2] Khushboo Suman,[3,4] Masoud Ghasemi,[5] Weiran Xie,[1] Ruiheng Wu,[2] Yuhang Wu,[1] Calvin L. Chao,[6] Julian E. Alberto,[3] Casey M. Lorch,[7] Ai-Nin Yang,[8] Dan My Nguyen,[8] Tulaja Shrestha,[8] Kayla Otero,[8] Chun-Yuan Lo,[8] Darrin Pochan,[1] Enrique D. Gomez,[5] Jonathan Rivnay,[2,9] Laure V. Kayser[1, 8]*

[1]*Department of Materials Science and Engineering, University of Delaware, Newark, DE 19716*
[2]*Department of Biomedical Engineering, Northwestern University, Evanston, IL, 60208*
[3]*Department of Chemical and Biomolecular Engineering, University of Delaware, Newark, DE 19716*
[4]*Department of Chemical Engineering, Indian Institute of Technology Madras, Chennai, India 600036*
[5]*Department of Chemical Engineering and Department of Materials Science and Engineering, the Pennsylvania State University, University Park, PA 16802*
[6]*Department of Surgery, Northwestern University Feinberg School of Medicine, Chicago, IL, 60611*
[7]*Department of Biomedical Engineering, University of Delaware, Newark, DE 19716*
[8]*Department of Chemistry and Biochemistry, University of Delaware, Newark, DE 19716*
[9]*Department of Materials Science and Engineering, Northwestern University, Evanston, IL 60208*
*Corresponding author. Email: lkayser@udel.edu

ABSTRACT

Electrically conductive hydrogels based on conducting polymers have found increased use in bioelectronics due to their low moduli that mimic biological tissues, their ability to transport both ionic and electronic charges, and their ease of processing in various form factors via printing or injection. Current approaches towards conductive hydrogels, however, rely on covalent and therefore irreversible crosslinking mechanisms. Here, we report a thermo-responsive conducting polymer (TR-CP) that undergoes a fully reversible non-covalent crosslinking at 35 °C within less than a minute to form conductive hydrogels. The TR-CP is based on a block polyelectrolyte complex, that self-assembles into well-defined colloidal particles in water which undergo an isovolumetric sol-gel transition just below physiological temperature. The hydrogels have tunable mechanical properties in the 20 to 200 Pa range, are stable at various pH and salt conditions, self-healing, injectable, and biocompatible in vitro and in vivo. We demonstrate that the TR-CPs can be used to fabricate sensitive, conformal and reusable electrodes for surface electromyography. This unique material provides exciting opportunities for stimuli-responsive and adaptive bioelectronics.

INTRODUCTION

Conducting polymers such as polyaniline (PANI), polypyrrole (PPy), and poly(3,4-ethylene dioxythiophene):poly(styrene sulfonate) (PEDOT:PSS) are versatile materials across bioelectronic applications. They have gained significant attention for their relative softness compared with inorganic materials, ability to transport both electronic and ionic charges, and ease of fabrication via solution processing.[1] Particularly, their deployment as scaffolds and hydrogels has enabled unique interpenetration and integration with biological systems,[2–4] through the formation of electrically-conductive materials with properties typically only achievable in insulating polymers. These conductive hydrogels can have mechanical properties mimicking soft tissues, injectability, or adhesiveness, which makes them useful in soft electrodes for electromyography[5], wearable electrical stimulators, [6] cardiac monitoring,[7] in vivo nerve stimulation,[38] and neural recording.[9–11] The most common approaches to preparing these functional conductive hydrogels are (1) blending a conductive polymer with a non-conductive crosslinked hydrogel with the properties of interest,[12] (2) blending a conductive polymer with a hydrogel precursor then crosslinking the blend,[13,14] or (3) oxidatively polymerizing the conducting polymer in the hydrogel or its precursor solution.[15] While effective, all these approaches rely on covalent crosslinkers leading to the lack of reversibility in the gelation process. Recently, Pappa and coworkers reported an example of crosslinker-free gelation using a mixture of chitosan, gelatin, and PEDOT:PSS.[16] However, these blends are liquid at physiological temperature which limits their applicability in in vivo and in vitro bioelectronics.

Here, we achieved a reversible sol-gel transition in conductive polymers just below physiological temperature (35 °C) through a fundamentally different approach that does not rely on covalent crosslinkers nor composite blends. The key molecular design was the synthesis of a thermo-responsive block copolymer of PSS with poly(N-isopropylacrylamide) (PSS-*b*-PNIPAM) that was then used as a matrix to prepare PEDOT:PSS-*b*-PNIPAM polyelectrolyte complexes (**Fig. 1a**). Due to the block copolymer structure, these intrinsically thermo-responsive conducting polymers (TR-CP) showed self-assembly of well-defined and stable colloidal particles in water, that rapidly (< 1min) and reversibly formed a conductive hydrogel network above 35 °C. The TR-CP gels have good conductivity (~ 10 mS cm^{-1}) and are cytocompatible in vitro and in vivo as prepared or in composites. We show that the TR-CP are self-healing and injectable and demonstrate their utility as reusable electrodes for surface electromyography (s-EMG). Due to their stimuli-responsive

properties, tolerance to a range of pH and salt concentrations, and cytocompatibility, the TR-CP could be transformative for further bioelectronic applications such as adaptive, patternable, injectable and thermally degradable electrodes, scaffolds, and actuators.

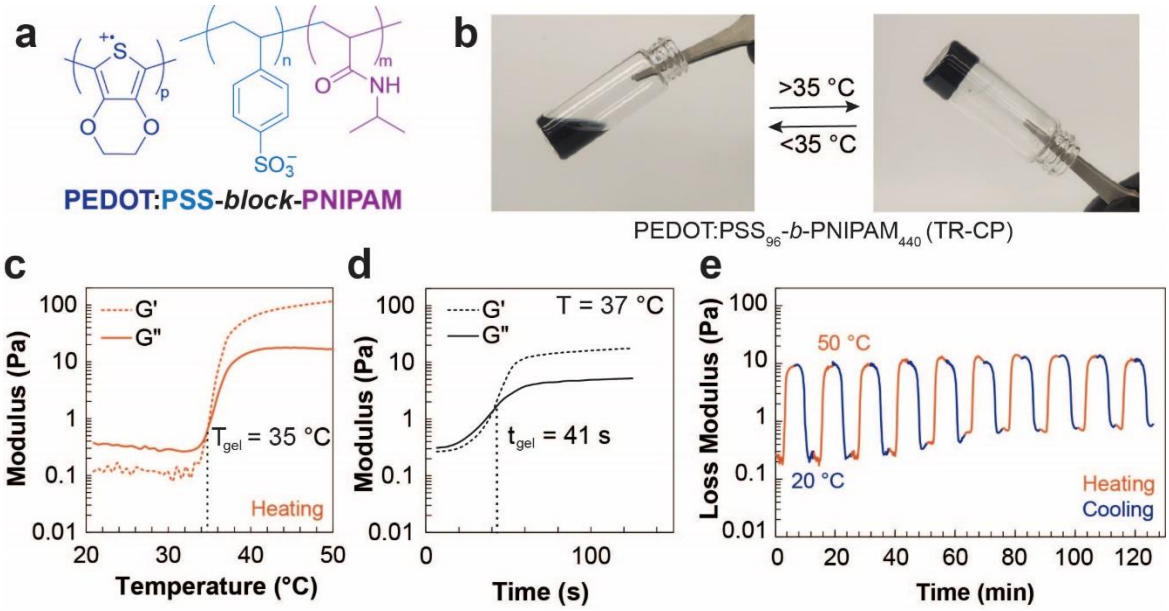

Fig. 1: Design and rheological properties of the thermo-responsive conductive polymers (TR-CP). **a.** Chemical structure of PEDOT:PSS-*b*-PNIPAM. **b.** Picture of the sol-gel transition in the TR-CP PEDOT:PSS$_{96}$-*b*-PNIPAM$_{440}$ at 35 °C (3.6 wt% in water). **c.** Variation in storage (G') and loss (G") moduli upon heating from 20 °C to 50 °C (5 °C/min). **d.** Change in storage (G') and loss (G") moduli as a function of time, at a constant temperature of 37 °C. **e.** Reversibility of the gelation and cycling stability over 10 heat-cool cycles from 20 °C to 50 °C on the rheometer.

Design, synthesis, and rheological properties of the TR-CP

To obtain TR-CP, we chose PEDOT:PSS as the conductive component because it is water-dispersible, oxygen stable, displays high conductivity in the solid state, and is readily used and studied in bioelectronics.[17] For the thermo-responsive component, PNIPAM was chosen because of its lower critical solution temperature (LCST) close to body temperature (32-35 °C).[18] To promote the phase separation of hydrophobic and hydrophilic domains and facilitate PNIPAM inter-chain interactions above the LCST to form gels, we synthesized **(Schemes S1-S2)** and characterized **(Fig. S1-S2)** block copolymers of PSS with PNIPAM with varying molecular weights and block ratio (**Table 1**) by reversible addition-fragmentation chain transfer (RAFT) polymerization (**SI, Section 3.1**). These block copolymers were then used as templates to

synthesize PEDOT:PSS-*b*-PNIPAM **(SI Scheme S3, Fig. 1a**) by oxidative polymerization of EDOT in water.

The phase change of these TR-CPs upon heating was monitored visually and by variable-temperature rheology (**Fig. S3**). We observed that the TR-CP with a mass ratio of PSS:PNIPAM of 1:2.3 (PEDOT:PSS_{96}-*b*-$PNIPAM_{440,}$ **Table 1**, **Entry 4**) formed a gel at T_{gel} = 35 °C (**Fig. 1b – c**) as estimated from the crossover point between the storage (G') and loss (G") moduli. The sol-gel transition was found to be isovolumetric (**Fig. S4a**) and very rapid, with a gelation time of only 41s at 37 °C (**Fig. 1d** and **Supplementary Video 1**). The storage modulus reached a plateau of 20 Pa at 37 °C, indicating the formation of a stable gel **(Fig. 1c)**. The gel was also stable over a wide range of frequencies at 37 °C from 0.1 rad s^{-1} to 20 rad s^{-1} (**Fig. S4b**). To establish the reversibility of the sol-gel transition, a subsequent cooling ramp was performed. We observed that on cooling below the LCST, the storage and loss moduli returned to their original values in the solution state, with a slight hysteresis **(Fig. S4c)**. Such hysteresis is observed commonly in other non-conductive thermo-responsive gels and can be eliminated by equilibration.[19,20] We established that the TR-CP retained its reversible sol-gel transition under multiple thermal cycling events as seen over ten heat-cool cycles in the rheometer (**Fig. 1e** and **Fig. S4d**). It was found that G" of the gel (50 °C) remained unchanged throughout the experiment. The storage modulus of the liquid increased slightly from 0.2 Pa to 0.4 Pa, likely caused by dehydration at prolonged exposure to temperatures above 40 °C. Anecdotally, we have performed more than these 10 thermal cycles in sealed vials without losing the reversible sol-gel transition.

Table 1. Synthesis of PSS-*b*-PNIPAM and thermo-responsive behavior of PEDOT:PSS-*b*-PNIPAM (TR-CP)

Entry	PSS-*b*-PNIPAM block copolymer	M_n PSS (kg mol^{-1})		$Đ^b$ PSS	M_n PSS-*b*-PNIPAM (kg mol^{-1})		$Đ^b$ PSS-*b*-PNIPAM	PSS:PNIPAM mass ratio[a]	Thermo-response of TR-CP at 37 °C [c]
		Theo.[a]	*Meas.*[b]		*Theo.*[a]	*Meas.*[b]			
1	PSS_{95}-*b*-$PNIPAM_{128}$	19.7	12.6	1.36	34.1	19.6	1.31	1:0.73	Increase in viscosity
2	PSS_{176}-*b*-$PNIPAM_{268}$	36.4	32.7	1.29	66.7	46.1	1.41	1:0.83	Increase in viscosity
3	PSS_{176}-*b*-$PNIPAM_{494}$	36.4	32.7	1.29	92.3	61.4	1.44	1:1.53	Weak gel
4	PSS_{96}-*b*-$PNIPAM_{440}$	19.9	14.5	1.27	69.6	41.2	1.20	1:2.3	Stable gel

[a] Determined by ^1H NMR in D_2O from monomer conversion. [b] Determined by gel permeation chromatography in DMF/water buffer 90:10 calibrated against PSSNa standards using a refractive index detector. [c] Molar ratio of PSS:PEDOT was held constant at 3.5:1.

Importantly, the TR-CP can be lyophilized and re-dispersed in aqueous solutions, including aqueous buffers of varying pH, PBS, or cell media, without affecting its reversible sol-gel transition. We re-dispersed the TR-CP in water at pH 7, and on changing the concentration from 3.6 wt% to 5.6 wt%, a negligible increase in T_{gel} was observed to 36 °C (**Fig. S5a**). However, the gelation time at 37 °C decreased to 23 s, and the storage modulus increased by an order of magnitude to 200 Pa (**Fig S5b**), highlighting the possibility to control gelation time and gel stiffness simply by changing the TR-CP concentration in water. TR-CP gels at both concentrations were stable for at least 15 min at 37 °C (**Fig. S5c**), and for several months in a closed vial at room temperature. The quick gelation time, tunable storage modulus and good stability under shear are all desirable for bioelectronics, particularly to interface with soft tissues.

To trigger a thermo-reversible gelation, we found that covalent functionalization of PEDOT:PSS with PNIPAM was necessary, as a control experiment showed that blending PEDOT:PSS with PNIPAM, as has been done in solid films,[21] resulted in only the precipitation of PNIPAM without gelation of PEDOT:PSS. We also found that the block copolymer structure is essential for the sol-gel transition. A random copolymer of PSS with PNIPAM (**Scheme S4**) used to prepare PEDOT:PSS-*co*-PNIPAM (**Scheme S5**), with identical mass ratios of all components as in the TR-CP, only displayed a slight increase in viscosity on heating. These control experiments highlight the need for a controlled block copolymer architecture to achieve the desired reversible gelation.

Electronic properties of the TR-CP

The electronic properties of TR-CP were investigated above and below the LCST using electrochemical impedance spectroscopy (EIS) (**Fig. S6a**). For the PEDOT:PSS_{96}-*b*-$PNIPAM_{440}$ TR-CP, upon increasing temperature, the Bode plot showed a decrease in the impedance magnitude indicative of an increase in conductivity upon gelation (**Fig. S6b**). To confirm this result, a modified Debye circuit model (**Fig. 2c**), commonly used for PEDOT:PSS-based hydrogels[22–24] was used to extract the electronic (R_e) and ionic (R_i) resistances (**Fig. S6c**). R_i for the liquid (86.8 Ω) and gel (121.7 Ω) were found to be similar. However, R_e decreased from 41.1 kΩ (liquid) to 22.5 kΩ (gel) on increasing temperature (**Table S1**). Next, we studied the effect of the PEDOT loading on the electronic properties of the TR-CP (**Fig. 2a-c**) to optimize for low impedance. The PSS:PEDOT molar ratio was changed to 3.5:1, 2.2:1 or 1.75:1 by changing the loading of EDOT during the oxidative polymerization. PSS:PEDOT = 3.5:1 was chosen as the

lower limit, as decreasing the loading of EDOT further only resulted in a slight increase in viscosity above the LCST, not gelation. At ratios higher than 1.75:1, the dispersions were not homogeneous at room temperature. We found that the 3.5:1 ratio showed the lowest impedance (**Fig. 2a**). From the equivalent circuit model (**Fig. 2c**), the ionic (σ_i) and electronic conductivity (σ_e) were calculated to be 34 mS cm^{-1} and 0.05 mS cm^{-1}, respectively (**Fig. 2b**). The TR-CP gel was incorporated into an electric circuit by depositing a liquid drop on a glass slide heated to 37 °C, demonstrating its ability to close a simple LED circuit upon gelation (**Fig 2d**).

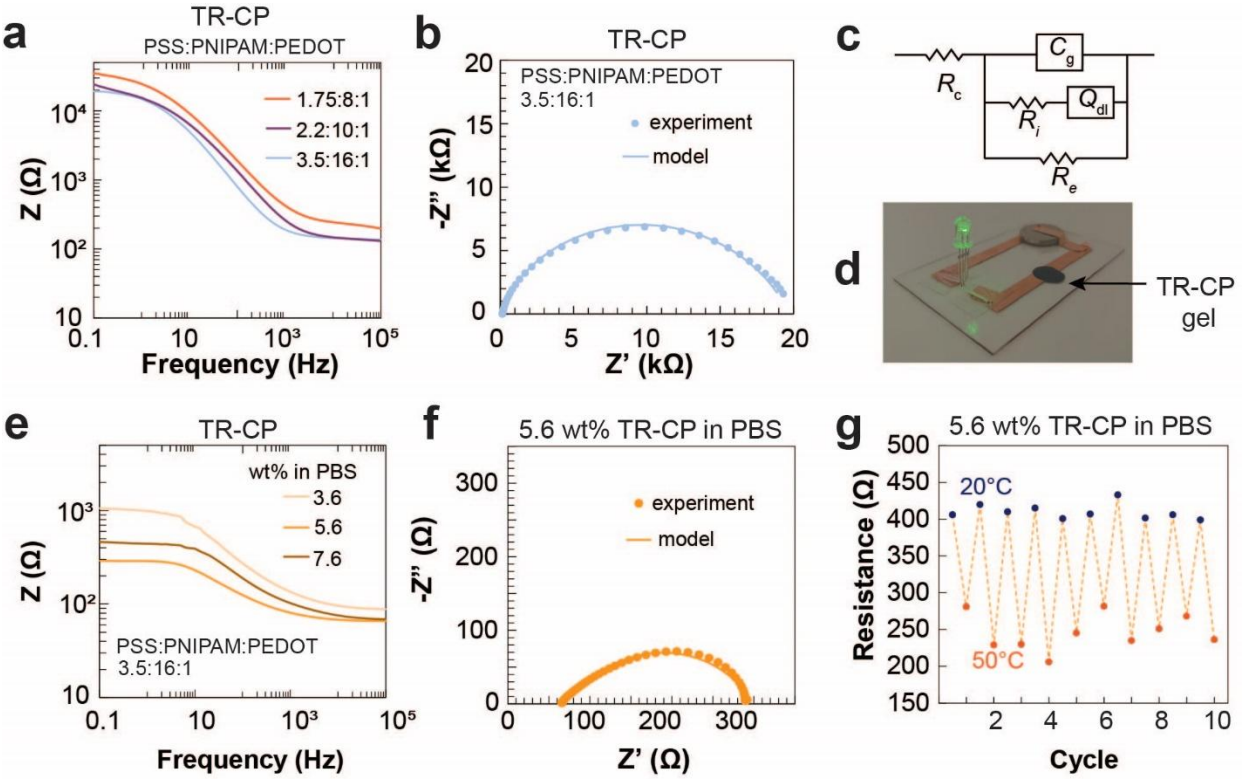

Fig. 2: Electronic properties of the PEDOT:PSS$_{96}$-*b*-PNIPAM$_{440}$ TR-CP. **a.** Bode plot obtained by EIS showing the effect of PEDOT loading on the impedance of the gels (3.6 wt% in DI water). **b.** Nyquist plot of the TR-CP with PSS:PNIPAM:PEDOT ratio of 3.5:16:1. **c.** Equivalent circuit model used to fit the EIS data and obtain ionic (R_i) and electronic (R_e) resistance. R_c is the charge transfer resistance, C_g is a constant phase element and Q_{dl} is a double-layer capacitor. **d.** Photograph showing an LED circuit completed with a TR-CP gel (PSS:PNIPAM:PEDOT ratio of 3.5:16:1, 3.6 wt% in DI water). **e.** Effect of TR-CP concentration in PBS (pH = 4) on the impedance magnitude. The TR-CP was lyophilized and re-dispersed at given concentrations in PBS. **f.** Nyquist plot for the TR-CP at 5.6 wt% in PBS (pH = 4) which showed the highest conductivity. **g**. Change in resistance (2-point probe DC measurements) as a function of temperature of the TR-CP (5.6 wt% in PBS, pH = 4) for a sample volume of 0.4 cm^3.

Lastly, we varied the concentration of the TR-CP thereby optimized with a PSS:PNIPAM:PEDOT ratio of 3.5:16:1, by reconstituting the lyophilized TR-CP in a phosphate-buffered saline (PBS) solution at different concentrations(**Fig. 2e**). As the concentration was increased from 3.6 wt% to 5.6 wt%, the 2-point probe DC conductivity increased from 2.1 mS cm^{-1} to 7.1 mS cm^{-1}. At 7.6 wt%, at which concentration the solution was very viscous and heterogeneous, the conductivity decreased to 5.5 mS cm^{-1}. The Nyquist plots for 3.6 wt% (**Fig. S7a**) and 5.6 wt% (**Fig. 2f**) displayed a smooth semi-circle, indicating good dispersion and homogeneity of the gel, while that of the 7.6 wt% TR-CP had irregular signals (**Fig. S7b**), further confirming that the gel was heterogenous leading to poor contact with the electrode. The fitting values of all circuit elements are tabulated in **Table S2** and calculated electronic and ionic conductivities are reported in **Table S3**. The highest conductivity recorded was for 5.6 wt% TR-CP (PSS:PNIPAM:PEDOT ratio of 3.5:16:1) in PBS: σ_i = 200 mS cm^{-1} and σ_e = 14 mS cm^{-1} from EIS (**Fig. 2f**) and σ = 10.4 mS cm^{-1} from 2-point probe, which is on par with other previously reported conductive hydrogels and sufficient for bioelectronic interfaces.[16,23,25] Finally, the reversibility of the electronic properties of this TR-CP formulation was evaluated by repetitively (10×) cycling the temperature between 50 ºC (gel) and 20 ºC (solution) while monitoring the electrical resistance. The gel displayed stable resistance values in both states upon multiple temperature cycles (**Fig. 2g**).

Microstructure and gelation mechanism

To characterize the microstructure and mechanism of gelation, microscopy and x-ray scattering techniques were employed. To elucidate the nanoscale structure of the TR-CP and what prompts it to form a porous network, we performed cryogenic transmission electron microscopy (cryo-EM) (**SI Section 3.4**). The samples were vitrified at two different temperatures, 25 °C and 45 °C, and two different concentrations, 1.8 wt% (no gelation observed, **Fig. S8**) and 3.6 wt% (gelation observed; **Fig. 3a-d**). For samples vitrified below the LCST (**Fig. 3a**, **3**c, **Fig. S9a**), the TR-CP at both concentrations exhibited structures with two different length scales: small spherical/ovoid particles with a radius of 4.7 ± 0.6 nm, sometimes assembled in a flexible chain—reminiscent of filomicelles—over 20 nm, and rod-like lamellar fringes predominantly outside these nanoparticles with close to 1.6 nm spacing (**Fig. S10, S11a, S11b**). These lamellar fringes are likely associated with a semi-crystalline PEDOT phase. The small size of these particles in solution likely explains

the excellent colloidal stability of the dispersion and their ability to be lyophilized and redispersed. For samples vitrified at 45 °C (above the LCST), cryo-EM showed significantly different structures depending on concentration. In the 1.8 wt% sample, we observed the formation of isolated spherical structures spaced about 50 nm apart (**Fig. S9b** and **S11c)**, while the 3.6 wt% samples showed the aggregation of the spherical particles leading to a bi-continuous phase with a mesh size of about 50 nm (**Fig. 3b**, **3d**, and **S11d**). In addition, cryo-EM micrographs of 1.8 wt% samples vitrified at 45 °C also showed the presence of lamellar fringes with ~1.6 nm spacing and small particles (~5 nm) in these samples (**Fig. S12**). These results show that although increasing the temperature caused the aggregation of the TR-CP colloids in both samples, only the 3.6 wt% samples met the criteria needed for gel formation. This observation is consistent with the visual inspection of the TR-CP and rheology, identifying 3.6 wt% as the lower limit of concentration for gel formation.

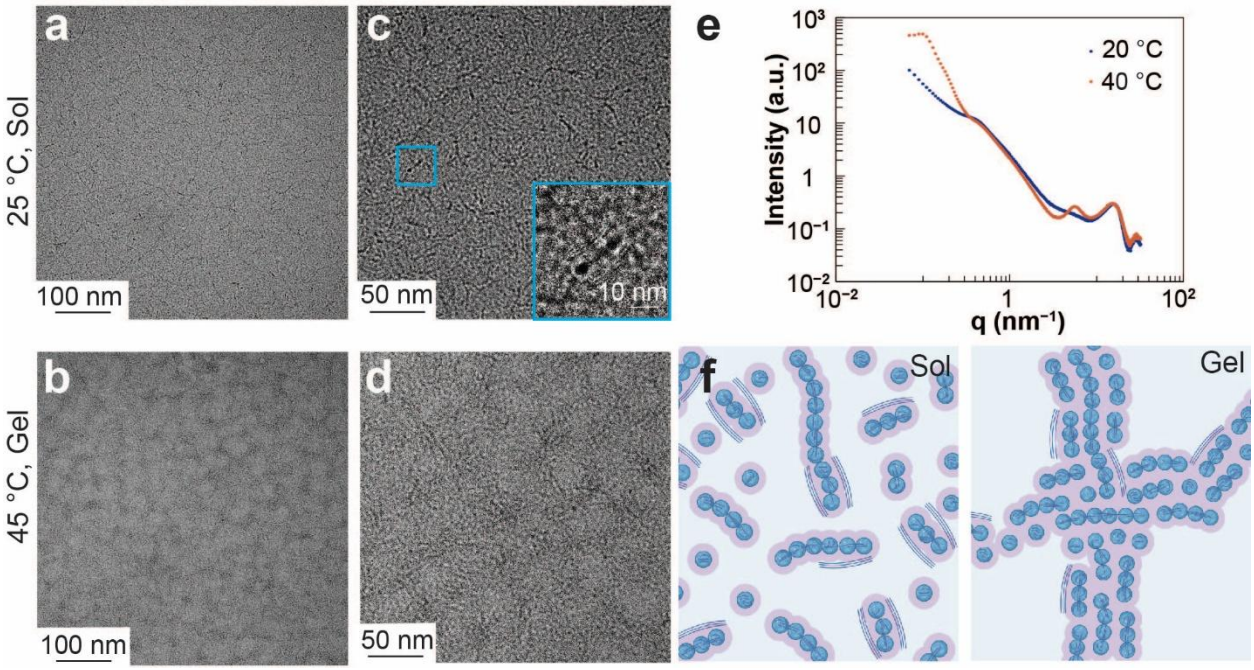

Fig. 3: Characterizing the microstructure and gelation mechanism of the PEDOT:PSS$_{96}$-*b*-PNIPAM$_{440}$ TR-CP (PSS:PEDOT molar ratio = 3.5:1). **a, c.** Cryo-EM images of 3.6 wt% TR-CP liquid below LCST, inset: lamellar fringes outside the colloidal particles. **b, d.** Cryo-EM images of 3.6 wt% TR-CP above LCST. **e.** Temperature-dependent small angle x-ray scattering (SAXS) of 3.6 wt% TR-CP in solution in water. **f.** Schematic of the self-assembled TR-CP colloids and proposed mechanism of gelation. Created using Biorender.com.

To confirm our observations from microscopy, small-angle X-ray scattering (SAXS) at 20 °C and 40 °C in solution was used to study the colloidal particle self-assembly, gel structure, and gelation mechanism (**Fig. 3e, SI Section 3.5**). Guinier-Porod model fitting[26] revealed that the TR-CP colloids in solution below the LCST are disk-shaped with a radius of around 5 nm and a disk thickness of 3.3-3.6 nm, consistent with the size of the spherical/ovoid nanoparticles seen by cryo-EM (**Fig. S13, Table S4**). As temperature increased above gelation, both the disk radius and thickness of these aggregates slightly increased. The intermediate q feature for single aggregate was slightly suppressed, while a strong structure factor peak S(q) appeared in low q range (centered at 0.102 nm^{-1}). These features indicate that after gelation, the particles aggregated to form large, ordered structures with a center-to-center distance of ~60 nm, in line with the cryo-EM results at 45 °C.

Based on these experiments, the following mechanisms for the formation of the particles and the gelation are proposed (**Fig. 3f**). During the oxidative polymerization of EDOT in the presence of PSS-*b*-PNIPAM (below the LCST), $PEDOT^+$ chains grow and complex with the PSS^- block. This polyelectrolyte complex is likely more hydrophobic than PNIPAM which results in the formation of spherical/ovoid particles with a PEDOT:PSS core and PNIPAM shell. The presence of PNIPAM in the shell is consistent with results from the surface elemental analysis by X-ray photoelectron spectroscopy (XPS), showing that the ratio of N:S is always higher (6.34 ± 0.36) than the theoretical N:S ratio of 4.5:1 (**Fig. S14**). In some cases, these disk-spheres are assembled in worm-like chains, likely through the polymerization of longer PEDOT chains within the core of the colloidal particles that forced the fusion of the spherical/ovoid particles. Occurrences of lamellar fringes outside the disk-spheres were seen on the cryo-EM, implying that some PEDOT also polymerized outside the shell and was electrostatically bound to the colloidal particles. Post-synthesis and above the LCST at a concentration of 3.6 wt%, the colloidal particles aggregate into a bi-continuous network while generally maintaining (or perhaps slightly increasing) their overall size, which leads to gelation. This aggregation can be attributed to inter-molecular hydrogen bonding of the PNIPAM domains above the LCST while the PEDOT:PSS core remained unchanged, consistent with results from Raman spectroscopy (**SI Section 3.7, Fig. S15, Table S5**). Overall, the block copolymer architecture of the PSS-*b*-PNIPAM was essential to achieving reversible gelation. It drove the self-assembly to colloids with the PNIPAM largely located at the surface, which ensured that the thermo-responsive PNIPAM was available for intermolecular

hydrogen bonding above its LCST leading to the formation of a colloidal network via non-covalent crosslinking.

In vitro and in vivo cytocompatibility of TR-CP and TR-CP/alginate composites

Biocompatibility is an important property of materials intended for bioelectronic and tissue engineering applications. The cytocompatibility of the TR-CP was assessed using the modified ISO 10993-5 protocol (**SI Section 3.8, 3.9**).[13] In addition to the pristine TR-CP, we also studied the cytocompatibility of TR-CP/alginate composites as a permanently crosslinked network would allow for more control in experiments (no need to constantly maintain T > LCST) and would allow for reliable gel identification in the in vivo studies. For these studies, we adjusted the TR-CP to a neutral pH. Characterization of the rheological (**Fig. S5a-c**) and electronic properties (**Fig. S16, Tables S6-S7)** show that the TR-CP behaves similarly under this pH and retains its sol-gel transition when reconstituted in cell media (**Fig. S17**).

To assess the in vitro cytotoxicity by indirect contact, alamarBlue™ assays were performed on extracts from the 3.6 wt% TR-CP gels (pH = 7, reconstituted in sterile cell media). L929 fibroblasts were cultured in the extracts and incubated for either 2 days or 7 days. Percent viability was calculated with respect to a sterilized cell culture media control. The day 1-5 extracts from the TR-CP all supported L929 fibroblasts well with high viability for both the 2-day (> 84%, **Fig. S18a**) and 7-day cultures (> 89%, **Fig. S18b**).

Next, a direct contact in vitro assay was performed (**Fig. 4a – c**) by suspending L929 fibroblasts in a media-reconstituted TR-CP dispersion before gelling. Collagen was used as a control and ethanol-treated collagen was used as a positive control. We saw high cell viability (> 95%, **Fig. 4a**) in the TR-CP gel (**Fig. S19a**). The control displayed larger cell spreading (**Fig. 4b**), potentially due to the stable gelation and structural integrity of the collagen, whereas cell culture in the pure 3.6% TR-CP resulted in less cell adhesion and spreading due to fluctuations in temperature during cell staining procedures (**Fig. 4c**). In preparation for in vivo studies, he TR-CPs were then incorporated into alginate precursor and subsequently chemically crosslinked, to form a permanently crosslinked TR-CP/alginate composite (**Fig. 4d – f, Fig. S20**). Direct contact viability was tested for TR-CP/alginate with two loadings of TR-CP in the composite (3.6 wt% and 5.6 wt%). Alginate treated with ethanol was used as a positive control (**Fig. S19b**). At both concentrations, no significant difference in cell viability was observed (**Fig. 4d**) between the

control alginate gel (**Fig. 4e**) and TR-CP/alginate gels (> 95%, **Fig. 4f** and **Fig. S19**). The positive cell outcomes of the TR-CP are consistent with prior reports of PEDOT:PSS composites containing PNIPAM,[27] and confirm the high in vitro cytocompatibility of the TR-CP. The rheological and electronic properties of TR-CP/alginate are summarized in **Fig. S21 - S22.** The samples and their controls for cytocompatibility are listed in **Table S8**.

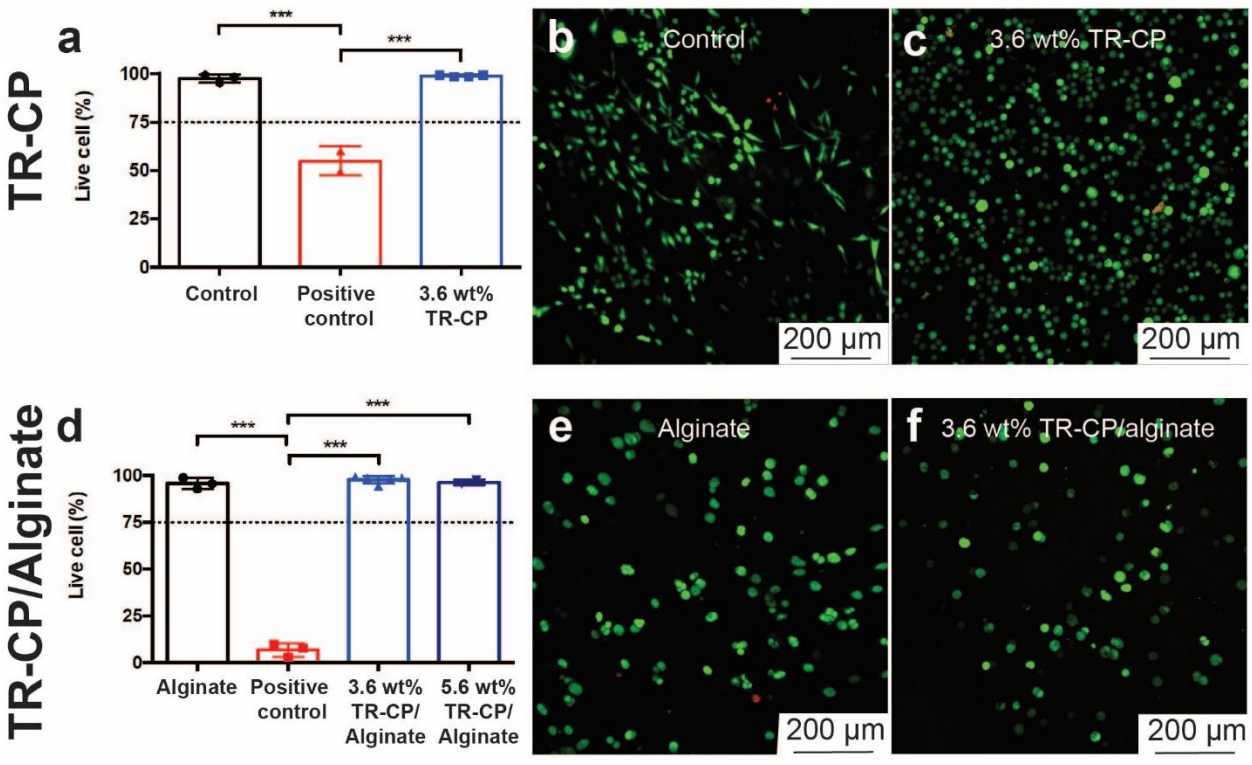

Fig. 4: Direct cytocompatibility assays with L929 fibroblast cells using fluorescence imaging with live/dead stains. Live cells fluoresce green (calcein-AM) while nuclei from dead cells fluoresce red (ethidium homodimer-1). **a.** Live cell % for 3.6 wt% TR-CP in PBS (pH = 7) compared to controls. The cells were incubated for 96 h for each group. **b.** Control: cells after incubating with control collagen gel; **c.** 3.6% TR-CP: cells after incubating with TR-CP. **d.** Live cell % for TR-CP/alginate composite. The cells were incubated for 48 h for each group. **e.** Control: cells after incubating with control alginate gel; **f.** 3.6 wt% TR-CP/alginate: Cells after incubating with 3.6% TR-CP in alginate gel.

To test the in vivo cytocompatibility of the TR-CP, permanently crosslinked 5.6 wt% TR-CP/alginate composite gels and control alginate gels were implanted subcutaneously into Sprague Dawley rats (**Fig. 5a – c**). The gels were explanted at 1- and 2-weeks post implantation to check for acute inflammatory response. At both time points, the rats showed no signs of distress, and the wound sites did not exhibit any signs of infection or hematoma. In both treatment groups, H&E staining revealed the intact gels surrounded by a layer of fascia residing beneath the muscle layer

of the skin (**Fig. 5d, e, g, h**). The connective tissue surrounding the TR-CP/alginate gels intimately interfaced with the gel (**Fig 5f**), though the thicker layer of tissue surrounding the TR-CP gel indicates a slightly increased inflammatory response compared to control. As others have observed, an increased inflammatory response is common when conducting polymers are implanted.[28,29] There were also signs of cell infiltration to the site of the gel, indicated by the presence of microvasculature in the surrounding tissue (**Fig. 5i**). Despite the increased cellular activity, the TR-CP did not cause any necrosis in the local skin environment. This study suggests the TR-CP/alginate composite gels have minimal negative effects to the overall tissue function, and while unoptimized, have potential as conductive biological interfaces.

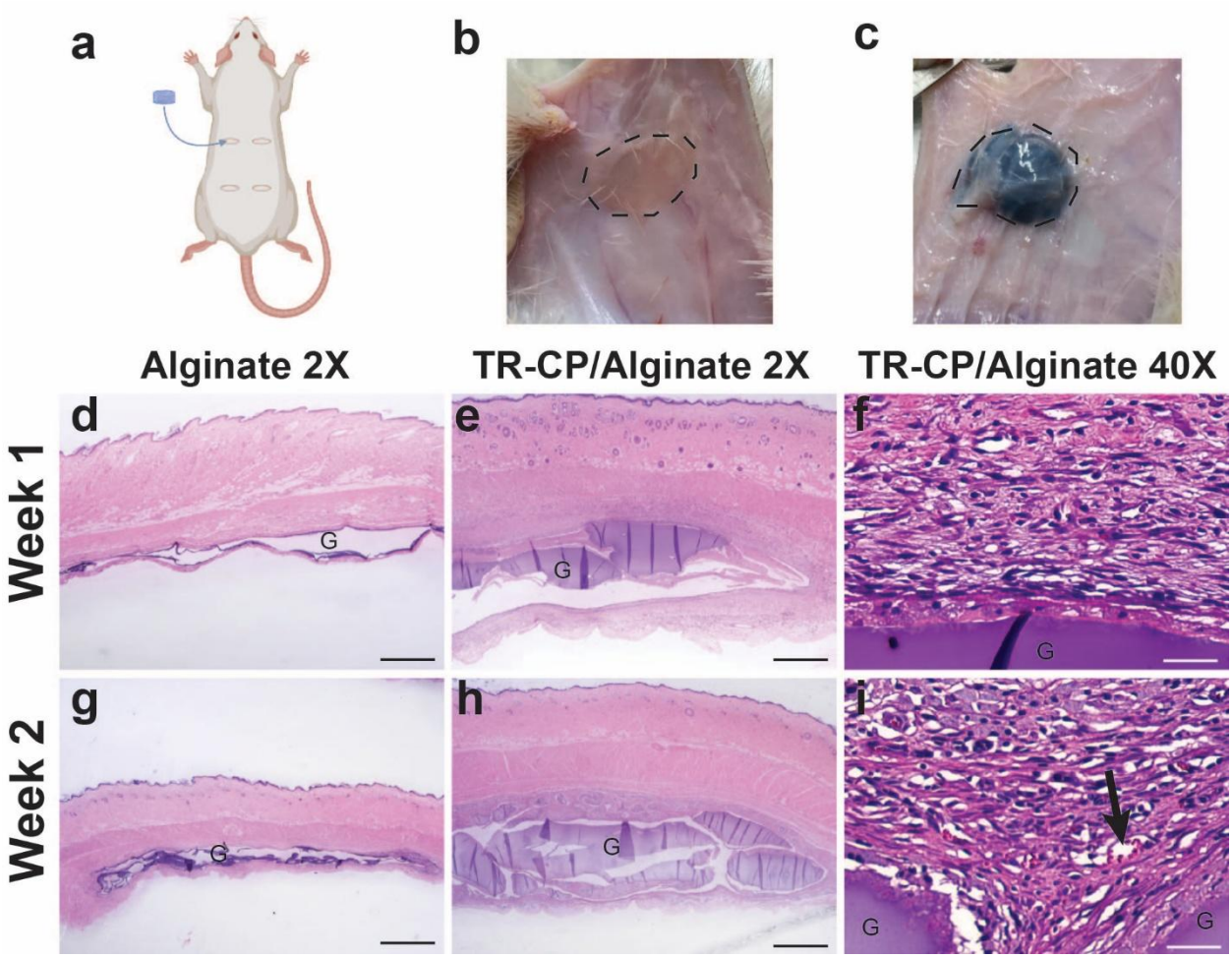

Fig. 5: Subcutaneous implantation in Sprague Dawley rats. **a.** Diagram of the placement of the subcutaneous pockets and gel implants. Photos of **b.** the alginate gel control and **c.** TR-CP/alginate composite gel in their subcutaneous pocket 2 weeks post implantation. **d – i.** Hematoxylin-eosin staining of skin sections with implanted gels at 1- and 2-weeks post implantation (G = gel; Arrow = microvasculature). Scale bar **d, e, g, h** = 1.5mm, **f, i** = 50 µm.

Processing of the TR-CP and demonstration as a reusable s-EMG electrode

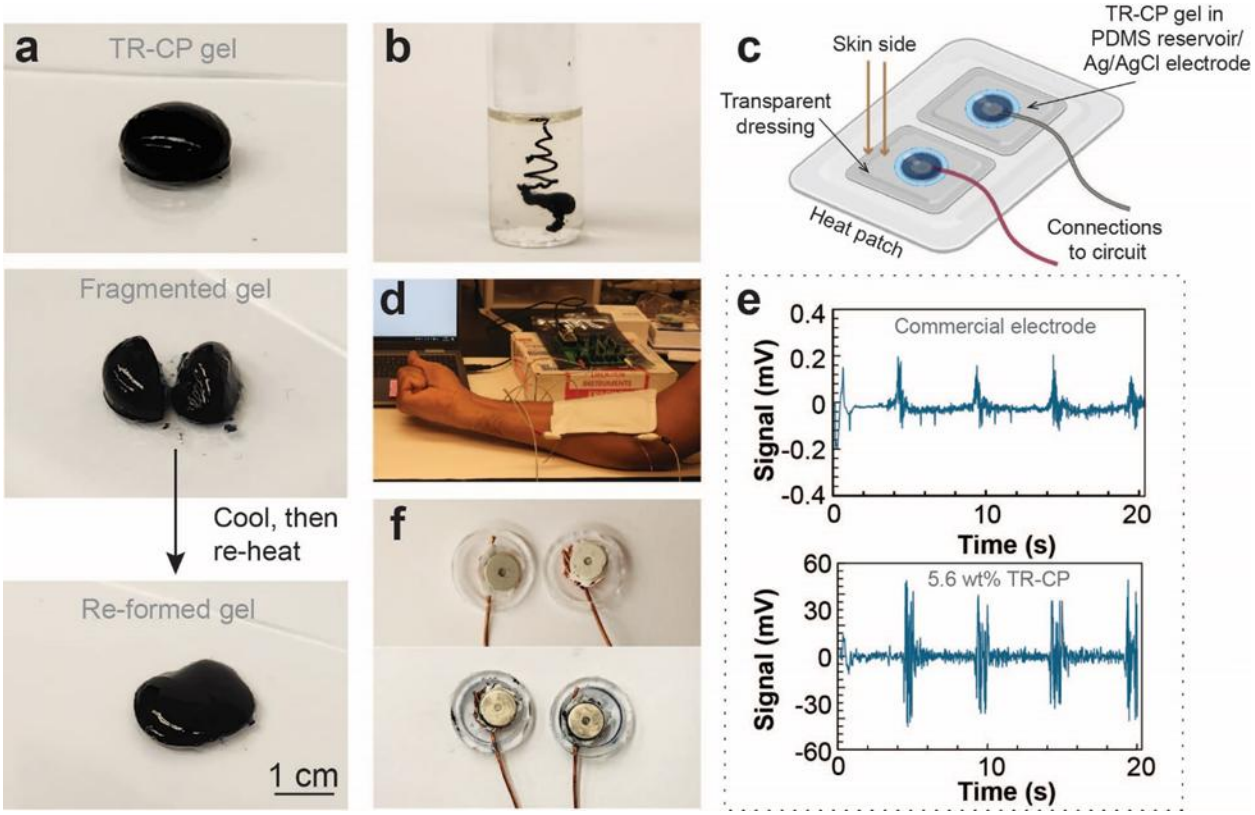

Fig. 6: Processing and example of application of the TR-CP. 5.6 wt% TR-CP in PBS at pH = 4 was used for all the experiments. **a.** Self-healing of the TR-CP. The TR-CP gel is formed by deposition on a heated glass slide, then cut and allowed to re-form by cooling slightly and re-heating. **b.** Picture of the TR-CP injected using a 21-gauge needle into a pre-heated alginate solution (1.8 wt% alginate in DI water, T = 37-40 °C). **c.** Schematic of the device for s-EMG measurements, created using Biorender.com. **d.** Picture of s-EMG set-up with TR-CPs, showing the connections and fist closing movement. **e.** Change in signal amplitude as a function of time, where each peak corresponds to fist closing and opening. **f.** Picture of s-EMG electrodes showing the Ag/AgCl connections and PDMS reservoirs for the TR-CP before and after use.

To explore the versatility of the TR-CP, we studied its processability by deposition on warm substrates or injection in warm fluids. First, we drop-casted 5.6 wt% TR-CP onto a glass slide heated to 37 °C **(Fig. 6a, Supplementary Video 2)**. The gel formed instantly on contact with the glass and assumed a hemispherical shape. The TR-CP gel was sliced with a razor blade, and the two halves maintained their shape well when kept at 37 °C. The gel was then allowed to cool to room temperature and was re-formed on heating the glass slide to 37 °C, thus displaying a self-healing behavior. Further, we investigated the injectability of TR-CPs into a warm, viscous alginate precursor solution (non-crosslinked) maintained at 37 °C (**Fig. 6b, Supplementary**

Video 3). The injected TR-CP gelled instantly, displayed minimal spreading, and stayed gelled as long as the temperature was maintained above 35 °C (**SI Section 3.12.2, Fig. S23**).

This behavior may be harnessed in future studies to make injectable conduits for electrical stimulation, 3D prints of functional materials and cell structures via support printing,[30,31] removable and conductive scaffolds for tissue engineering, or injectable microelectrode arrays for sensing and recording.[32,33]

Lastly, to demonstrate an application for the TR-CP, we developed a conformal and reusable surface electromyography (s-EMG) epidermal electrode (**Fig. 6c**). The TR-CP (5.6 wt% in PBS) was drop-casted into a soft PDMS reservoir and heated until gelation to form electrodes. The TR-CP device was adhered to skin using a transparent dressing, along with a heating patch to ensure a stable temperature throughout the experiment. The device was used to record fist closing and opening movements (**Fig. 6d, Supplementary Video 4**). We observed that in comparison to commercial electrodes, the TR-CP device displayed a higher signal amplitude (250×) with minimal parasitic noise (**Fig. 6e**). We attributed this performance enhancement to the mixed ionic-electronic conductivity of the TR-CP and shape-conforming behavior due to its soft and adaptable mechanics. The low modulus of this soft electronic interface prevented any discomfort on skin and provided good conformal contact throughout the measurement. Post-recording, the electrodes were cooled down and TR-CP liquid was extracted, thus demonstrating the reusability of the TR-CPs (**Fig. 6f**) and their potential for use as shape-conforming bioelectronic interfaces which could be harnessed for measurements on non-uniform surfaces such as hairy skin.

Conclusions and outlook

In this study, we developed intrinsically thermo-responsive and conductive polymers (TR-CPs) with a fully reversible sol-gel transition to circumvent the need for covalent and irreversible crosslinking in conductive hydrogels. We leveraged the self-assembly of block polyelectrolyte complexes to achieve stable and well-defined colloids. Above the transition temperature (35-36 °C), dispersions of the TR-CP undergo a very rapid (< 1 min) and isovolumetric gelation under a range of pH and ionic environments, resulting from the aggregation of the colloids into a bi-continuous network. These gels are electrically conductive and cytocompatible, and therefore amenable to applications in bioelectronics, which we demonstrated in a conformal and reusable surface electromyography device.

The molecular design introduced in this study may inform the development of organic conductors for applications in bioelectronics and beyond. Block copolymers could be used to tune the viscosity of PEDOT:PSS derivatives for injection 2D and 3D printing or adding other functionalities than thermo-responsiveness such as adhesiveness, analyte selectivity and biodegradation, which we will study in the future. From a bioelectronics perspective, we envision the TR-CP to find use in a range of different applications. For example, their high conformability and hydration would improve interfacing with uneven and oddly shaped substrates, such as hairy skin, scalp and irregularly shaped wounds. For in vitro bioelectronics requiring phenotyping studies after encapsulation, the de-crosslinking of the gels upon cooling may enable easy recovery of the biological substrate while preventing tissue or cell damage. Lastly, the thermo-response also enables injectability from very fine needles without applying excessive shear stress which may be beneficial for injectable scaffolds, electrodes, and bioprinting with high precision.

Author contributions

V. S. D. and L. V. K. conceived the project and designed the experiments. V. S. D. synthesized the materials. X. X. performed in vitro cytocompatibility experiments and analyzed the data. R. D. and C. C. performed in vivo biocompatibility experiments and analyzed the data. V. S. D. and K. S. designed and performed rheology experiments and analyzed the data. M. G. performed the cryo-EM experiments and M. G. and E. D. G. analyzed the data. W. X. performed the SAXS experiments. R. W. modelled and analyzed the SAXS data. V. S. D., Y. W. and C. Y. L. performed electronics measurements and analysis. J. A., C. L. and A. N. Y. assisted with the materials synthesis. T. S. performed XPS experiments and helped V. S. D. with data analysis. K. O. and V. S. D. performed in-situ Raman experiments and analyzed the data. V. S. D. designed and developed the s-EMG electrodes. D. M. N. and V. S. D. performed the s-EMG experiments and analyzed the data. D. P., E. D. G., J. R., and L. V. K. provided guidance and funding. All authors contributed to writing and editing the manuscript.

Acknowledgements

This work was supported by a National Science Foundation (NSF) CAREER award (grant No. DMR-2237888), a Beckman Young Investigator award from the Arnold and Mabel Beckman Foundation, and a University of Delaware Research Foundation (UDRF) seed funding to L.V.K. X. X. and J. R. acknowledge support from the Army Research Office under Cooperative

Agreement Number W911NF-23-2-0138. The views and conclusions contained in this document are those of the authors and should not be interpreted as representing the official policies, either expressed or implied, of the Army Research Office or the U.S. Government. The U.S. Government is authorized to reproduce and distribute reprints for Government purposes notwithstanding any copyright notation herein. R. D. and J. R. acknowledge support from NIH grant 5T32EB031527-04. K. S. acknowledges funding support from National Institute of Standards and Technology (NIST), Department of Commerce under agreement #370NANB17H302. W. X. and D. P. acknowledge support by NSF through the University of Delaware Materials Research Science and Engineering Center (MRSEC) (DMR-2011824). M. G. and E. D. G. acknowledge support from NSF under Award DMR-1905550. C. L. C. acknowledges support from NIH grant 5T32EB031527-04. The use of facilities and instrumentation at the University of Delaware was supported by the National Institutes of Health (NIH), NSF awards CHE-0421224 (NMR), and CHE-1428149 (XPS). SAXS experiments were performed at the LiX beamline of the National Synchrotron Light Source II, a U.S. Department of Energy (DOE) Office of Science User Facility operated for the DOE Office of Science by Brookhaven National Laboratory under Contract No. DE-SC0012704. The LiX beamline is part of the Center for BioMolecular Structure (CBMS) which is primarily supported by the NIH NIGMS through a Center Core P30 Grant (P30GM133893), and by the DOE Office of Biological and Environmental Research (KP1607011). The authors would like to thank Prof. Norman Wagner for access to the AR-G2 rheometer, Prof. Emil Hernandez-Pagan for access to the in-situ Raman spectrometer, and Prof. David Martin for access to electronic characterization equipment. We would also like to thank Tulika Bhattacharya for her help in conducting rheology experiments, and Yaping Wang and Yong Zhao for their help in collecting preliminary data for TEM and cryo-EM.

Financial competing interest

The authors declare no competing financial interest. A patent filed by the University of Delaware (PCT International Patent Application No. PCT/US2023/015527) is pending for the TR-CP.

References

1. Someya, T., Bao, Z. & Malliaras, G. G. The rise of plastic bioelectronics. *Nature* **540**, 379–385 (2016).

2. Yang, M. *et al.* Robust Neural Interfaces with Photopatternable, Bioadhesive, and Highly Conductive Hydrogels for Stable Chronic Neuromodulation. *ACS Nano* **17**, 885–895 (2023).
3. Yang, M. *et al.* Highly-stable, injectable, conductive hydrogel for chronic neuromodulation. *Nat. Commun.* **15**, 7993 (2024).
4. Yan, M. *et al.* Conducting Polymer-Hydrogel Interpenetrating Networks for Improving the Electrode-Neural Interface. *ACS Appl. Mater. Interfaces* **15**, 41310–41323 (2023).
5. Chong, J. *et al.* Highly conductive tissue-like hydrogel interface through template-directed assembly. *Nat. Commun.* **14**, 2206 (2023).
6. Lim, C. *et al.* Tissue-like skin-device interface for wearable bioelectronics by using ultrasoft, mass-permeable, and low-impedance hydrogels. *Sci. Adv.* **7**, eabd3716 (2021).
7. Deng, J. *et al.* A bioadhesive pacing lead for atraumatic cardiac monitoring and stimulation in rodent and porcine models. *Sci. Transl. Med.* **16**, eado9003 (2024).
8. Strakosas, X. *et al.* Metabolite-induced in vivo fabrication of substrate-free organic bioelectronics. *Science* **379**, 795–802 (2023).
9. Won, D. *et al.* Digital selective transformation and patterning of highly conductive hydrogel bioelectronics by laser-induced phase separation. *Sci. Adv.* **8**, 3209 (2022).
10. Zhang, J. *et al.* Engineering Electrodes with Robust Conducting Hydrogel Coating for Neural Recording and Modulation. *Adv. Mater.* **35**, 2209324 (2023).
11. Dong, C. *et al.* Electrochemically actuated microelectrodes for minimally invasive peripheral nerve interfaces. *Nat. Mater.* **23**, 969–976 (2024).
12. Ji, D. *et al.* Superstrong, superstiff, and conductive alginate hydrogels. *Nat. Commun.* **13**, 3019 (2022).
13. Tropp, J. *et al.* Conducting Polymer Nanoparticles with Intrinsic Aqueous Dispersibility for Conductive Hydrogels. *Adv. Mater.* **36**, 2306691 (2024).
14. Lopez-Larrea, N. *et al.* PNIPAM/PEDOT:PSS Hydrogels for Multifunctional Organic Electrochemical Transistors. *Adv. Funct. Mater.* **34**, 2403708 (2024).
15. Nguyen, D. M. *et al.* Electronically Conductive Hydrogels by in Situ Polymerization of a Water-Soluble EDOT-Derived Monomer. *Adv. Eng. Mater.* **24**, 2200280 (2022).
16. Alsaafeen, N. B. *et al.* One-Pot Synthesis of a Robust Crosslinker-Free Thermo-Reversible Conducting Hydrogel Electrode for Epidermal Electronics. *ACS Appl. Mater.*

Interfaces (2024) doi:https://doi.org/10.1021/acsami.3c10663.

17. Seiti, M., Giuri, A., Corcione, C. E. & Ferraris, E. Advancements in tailoring PEDOT: PSS properties for bioelectronic applications: A comprehensive review. *Biomater. Adv.* **154**, 213655 (2023).
18. Lanzalaco, S. & Armelin, E. Poly(N-isopropylacrylamide) and Copolymers: A Review on Recent Progresses in Biomedical Applications. *Gels* **3**, 36 (2017).
19. Gordon, M. B., Kloxin, C. J. & Wagner, N. J. The rheology and microstructure of an aging thermoreversible colloidal gel. *J. Rheol.* **61**, 23–34 (2017).
20. Suman, K. & Wagner, N. J. Anomalous rheological aging of a model thermoreversible colloidal gel following a thermal quench. *J. Chem. Phys.* **157**, 024901 (2022).
21. Garcia-Hernando, M. *et al.* An electroactive and thermo-responsive material for the capture and release of cells. *Biosens. Bioelectron.* **191**, 113405 (2021).
22. Feig, V. R., Tran, H., Lee, M. & Bao, Z. Mechanically tunable conductive interpenetrating network hydrogels that mimic the elastic moduli of biological tissue. *Nat. Commun.* **9**, 2740 (2018).
23. Nguyen, D. M. *et al.* One Pot Photomediated Formation of Electrically Conductive Hydrogels. *ACS Polym. Au* **4**, 34–44 (2024).
24. Lu, B. *et al.* Pure PEDOT:PSS hydrogels. *Nat. Commun.* **10**, 1043 (2019).
25. Aydemir, U. *et al.* In situ assembly of an injectable cardiac stimulator. *Nat. Commun.* **15**, 6774 (2024).
26. Beaucage, G. & Schaefer, D. W. Structural studies of complex systems using small-angle scattering: a unified Guinier/power-law approach. *J. Non. Cryst. Solids* **172**–**174**, 797–805 (1994).
27. Sharma, A. K., Sharma, Y. & Duhan, S. Biocompatible Smart Matrices Based on Poly (3,4-ethylenedioxythiophene) - Poly (N-isopropylacrylamide) Composite. *Int. J. Polym. Mater. Polym. Biomater.* **64**, 333–337 (2015).
28. Sun, K. H. *et al.* Evaluation of in vitro and in vivo biocompatibility of a myo-inositol hexakisphosphate gelated polyaniline hydrogel in a rat model. *Sci. Rep.* **6**, 23931 (2016).
29. Rivers, T. J., Hudson, T. W. & Schmidt, C. E. Synthesis of a Novel, Biodegradable Electrically Conducting Polymer for Biomedical Applications. *Adv. Funct. Mater.* **12**, 33–37 (2002).

30. Hinton, T. J. *et al.* Three-dimensional printing of complex biological structures by freeform reversible embedding of suspended hydrogels. *Sci. Adv.* **1**, e1500758 (2015).
31. Xie, X. *et al.* Liquid-in-liquid printing of 3D and mechanically tunable conductive hydrogels. *Nat. Commun.* **14**, 4289 (2023).
32. Spencer, A. R. *et al.* Bioprinting of a Cell-Laden Conductive Hydrogel Composite. *ACS Appl. Mater. Interfaces* **11**, 30518–30533 (2019).
33. Athukorala, S. S. *et al.* 3D Printable Electrically Conductive Hydrogel Scaffolds for Biomedical Applications: A Review. *Polymers* **13**, 474 (2021).